DA-Raf–dependent inhibition of the Ras-ERK signaling pathway in type 2 alveolar epithelial cells controls alveolar formation

Haruko Watanabe-Takano[a,b,c,1], Kazunori Takano[b,d], Akemi Sakamoto[e], Kenji Matsumoto[f], Takeshi Tokuhisa[e], Takeshi Endo[b,d,2], and Masahiko Hatano[a,2]

Departments of [a]Biomedical Science and [e]Developmental Genetics, Graduate School of Medicine, Chiba University, Inohana, Chuo-ku, Chiba 260-8670, Japan; [b]Department of Biology, Graduate School of Science and [d]Graduate School of Advanced Integration Science, Chiba University, Yayoicho, Inage-ku, Chiba 263-8522, Japan; [c]Japan Society for the Promotion of Science, Chiyoda-ku, Tokyo 102-0083, Japan; and [f]Department of Allergy and Immunology, National Research Institute for Child Health and Development, Setagaya-ku, Tokyo 157-8535, Japan

Edited by Ewald R. Weibel, University of Bern, Switzerland, and approved April 18, 2014 (received for review December 2, 2013)

Alveolar formation is coupled to the spatiotemporally regulated differentiation of alveolar myofibroblasts (AMYFs), which contribute to the morphological changes of interalveolar walls. Although the Ras-ERK signaling pathway is one of the key regulators for alveolar formation in developing lungs, the intrinsic molecular and cellular mechanisms underlying its role remain largely unknown. By analyzing the Ras-ERK signaling pathway during postnatal development of lungs, we have identified a critical role of DA-Raf1 (DA-Raf)—a dominant-negative antagonist for the Ras-ERK signaling pathway—in alveolar formation. DA-Raf–deficient mice displayed alveolar dysgenesis as a result of the blockade of AMYF differentiation. DA-Raf is predominantly expressed in type 2 alveolar epithelial cells (AEC2s) in developing lungs, and DA-Raf–dependent MEK1/2 inhibition in AEC2s suppresses expression of tissue inhibitor of matalloprotienase 4 (TIMP4), which prevents a subsequent proteolytic cascade matrix metalloproteinase (MMP)14–MMP2. Furthermore, MMP14–MMP2 proteolytic cascade regulates AMYF differentiation and alveolar formation. Therefore, DA-Raf–dependent inhibition of the Ras-ERK signaling pathway in AEC2s is required for alveolar formation via triggering MMP2 activation followed by AMYF differentiation. These findings reveal a pivotal role of the Ras-ERK signaling pathway in the dynamic regulation of alveolar development.

Alveoli are the basic units of gas exchange that are essential for maintaining life in air-breathing vertebrates. To expand the surface area for gas exchange, immature prealveolar saccules in neonates are subdivided into alveoli by the formation of new alveolar septa (secondary septation) within few weeks after birth. Immature prealveolar saccules mainly contain two types of alveolar epithelial cells (AECs). Type 1 AECs (AEC1s), which are flat and occupy the large part of alveolar surface, are involved in gas exchange, whereas type 2 AECs (AEC2s), which are small and cuboidal cells, secrete surfactants to lower the surface tension of lungs (1, 2). During secondary septation, alveolar myofibroblast (AMYF) precursors expressing platelet-derived growth factor-receptor-α subunit (PDGFRα) are induced by epithelial-derived PDGF-A and differentiate into AMYFs (3–6). AMYFs expressing contractile α-smooth muscle actin (α-SMA) transiently appear at the tips of the new alveolar septa from postnatal day (P) 5 and deposit extracellular matrix (ECM) proteins, including tropoelastin, collagen, and fibronectin, which provide the driving force for folding up of interalveolar walls (7–9). Accumulating evidence also suggests that secondary septation is a highly complicated process regulated by multiple microenvironmental cues, such as direct cell–cell interaction, paracrine signals, and ECM contact. In particular, ECM proteins and their remodeling enzymes, including matrix metalloproteinase (MMP)2 and MMP14 (also known as MT1-MMP), are important in both providing the scaffolds and determining the bioavailability of diverse ligands for alveolar morphogenesis (10–13).

The Ras-ERK signaling pathway is one of the key regulators for not only tracheal branching but also alveolar formation in developing lungs (14–16). The Ras-ERK signaling pathway transmits extracellular stimuli from the plasma membrane to the cytoplasm or the nucleus (17–19). Following receptor autophosphorylation, Ras proteins (H-Ras, N-Ras, and K-Ras) are activated in the plasma membrane and consequently recruit Raf family serine/threonine kinases (A-Raf, B-Raf, and C-Raf) via their conserved Ras-binding domain. Then, the activated Raf kinases induce serial phosphorylation and activation of MEK1/2 and ERK1/2 to regulate transcription factors. We have identified DA-Raf as a splicing variant of A-Raf (20). DA-Raf shares a common Ras-binding domain with A-Raf, but lacks the kinase domain. As expected from its domain structure, DA-Raf binds to the activated Ras proteins and inhibits the activation of downstream kinases, MEK1/2 and ERK1/2, in vitro.

Although the Ras-ERK signaling pathway is one of the key regulators for alveolar formation in developing lungs, the molecular and cellular mechanisms underlying its role remain

Significance

Alveoli participating in gas exchange are essential for maintaining life in air-breathing vertebrates. In developing lungs, alveolar myofibroblasts (AMYFs) cause morphological changes of interalveolar walls and consequently generate alveoli. Although the Ras-ERK signaling pathway is known to regulate alveolar formation, the molecular and cellular mechanisms underlying its role remain largely obscure. Here, we clarified a critical role of DA-Raf1 (DA-Raf)—a dominant-negative antagonist of the Ras-ERK signaling pathway—in alveolar formation. DA-Raf–deficient mice displayed alveolar dysgenesis resulting from defective AMYF differentiation. DA-Raf–dependent MEK1/2 inhibition in type 2 alveolar epithelial cells induces activation of matrix metalloproteinases, which is required for AMYF differentiation. Our findings reveal a pivotal role of DA-Raf–mediated regulation of the Ras-ERK signaling pathway in alveolar formation.

Author contributions: H.W.-T., T.T., T.E., and M.H. designed research; H.W.-T., K.T., A.S., and K.M. performed research; H.W.-T. and K.T. analyzed data; and H.W.-T., T.T., T.E., and M.H. wrote the paper.

The authors declare no conflict of interest.

This article is a PNAS Direct Submission.

Freely available online through the PNAS open access option.

[1]Present address: Department of Cell Biology, National Cerebral and Cardiovascular Center Research Institute, Suita, Osaka 565-8565, Japan.

[2]To whom correspondence may be addressed. E-mail: t.endo@faculty.chiba-u.jp or hatanom@faculty.chiba-u.jp.

This article contains supporting information online at www.pnas.org/lookup/suppl/doi:10.1073/pnas.1321574111/-/DCSupplemental.

largely unknown. Here, we show that DA-Raf–dependent suppression of the Ras-ERK signaling pathway in AEC2s non–cell-autonomously promotes AMYF differentiation and alveolar formation through the transcriptional control of *tissue inhibitor of metalloproteinase 4* (*Timp4*), which prevents a subsequent proteolytic cascade MMP14–MMP2. These findings provide novel insight into mechanisms of alveolar formation linking the role of the Ras-ERK signaling pathway in AEC2s to the AMYF differentiation, and may contribute to develop regeneration therapies for chronic obstructive pulmonary disease (COPD) by inducing the recapitulation of alveolar development.

Results

DA-Raf–Deficient Mice Have Defective Alveolar Formation. To examine the activation levels of the Ras-ERK signaling pathway, we first analyzed the amounts of phosphorylated MEK1/2 during postnatal stages of lungs in WT C57BL/6 mice. Western blot analysis showed gradually declining levels of phosphorylated MEK1/2 from P2 to P14 along with the progression of lung development (Fig. 1*A*). Therefore, we analyzed the expression levels of DA-Raf and other negative regulators of the Ras-ERK signaling pathway, such as Sprouty and Spred families. We found that the levels of DA-Raf expression and binding between Ras proteins and DA-Raf were inversely correlated with the activation status of the Ras-ERK signaling pathway (Fig. 1*A* and Fig. S1). In contrast, both the amounts of other Raf family proteins and gene-expression levels of other negative regulators were nearly constant in the lungs until P14 (Fig. 1*A* and Fig. S1*B*).

To determine the role of DA-Raf in developing lungs, we generated DA-Raf–deficient mice without affecting A-Raf expression in embryonic stem (ES) cells by targeting the DNA region including introns 6 and 7, which contain the stop sequences for *DAraf* transcription (Fig. S2 *A* and *B*). Mating of DA-Raf heterozygous female (X^-/X) mice with WT C57BL/6 male (X/Y) mice resulted in offspring at the expected Mendelian ratio, and the overall sex ratio was close to 1:1. Western blotting showed specific ablation of DA-Raf without affecting A-Raf expression in the brains of DA-Raf–deficient male (X^-/Y) mice (Fig. S2*C*). However, more than 50% of X^-/Y mice died within the first week after birth and the rest died by ∼3 wk of age (Fig. S2*D*). Furthermore, the growth curves of X^-/Y and X^-/X mice were significantly slower than sex-matched littermates (Fig. S2*E*), suggesting abnormalities in both X^-/Y and X^-/X mice during postnatal development.

As expected, we found dysgenesis in the lungs of X^-/Y mice (Fig. 1*B* and Fig. S2*F*). Although there were no abnormalities in lungs of X^-/Y mice until P2, the parenchyma in lungs of X^-/Y mice became thinner and flatter compared with their X/Y littermates from P5. Many alveolar septa extended from prealveolar saccules gave rise to alveoli in the lungs of X/Y mice from P7 to P14; however, there were few alveolar septa in X^-/Y mice. Morphometric analysis of developing lungs revealed significant reductions in both lung volumes and alveolar numbers per lung in X^-/Y mice from P5 to P14 compared with control mice (Fig. 1*C* and Fig. S2*G*). Whereas alveolar numbers per unit lung volume significantly increased from P2 to P5 in X/Y mice, they remained unchanged in X^-/Y mice until P14 (Fig. 1*D*), suggesting defective secondary septation in X^-/Y mice. Furthermore, the values of lung volume per body weight were comparable between X/Y and X^-/Y mice from P2 to P14 (Fig. S2*H*), indicating that the components of alveolar units are normally added in X^-/Y mice during postnatal lung growth. These findings demonstrate that the secondary septation is seriously defective in X^-/Y mice during postnatal development.

Differentiation of AMYFs Is Blocked During Alveolar Formation in DA-Raf–Deficient Mice. It has been shown that AMYFs are involved in the secondary septation (7, 8). To clarify whether AMYFs develop normally in X^-/Y mice, we conducted immunostaining for α-SMA, which is specifically expressed in smooth muscle cells (SMCs) and myofibroblasts. Although AMYFs transiently appeared in the lungs of X/Y mice from P5 to P7, the number of these cells in X^-/Y mice was extremely reduced (Fig. 2*A*). In contrast, SMCs in vascular and bronchial regions and resident myofibroblasts (RMYFs) in the lungs of X^-/Y mice were comparable to those of X/Y mice (Fig. 2*A* and Fig. S3*A*). Thus, to determine whether AMYF precursors are also impaired in the lungs of X^-/Y mice, we next analyzed PDGFRα$^+$ cells in developing lungs. Immunohistochemical analysis further confirmed an extensive increase of PDGFRα$^+$/α-SMA$^+$ cells at the tips of alveolar septa in X/Y mice from P2 to P7 (Fig. S3*B*), which indicates that these cells were AMYFs. Flow cytometric measurement revealed that the fraction of AMYFs from X^-/Y mice was dramatically reduced to about one-fourth the level in X/Y littermates at P6 (Fig. 2 *B* and *C*). Conversely, the percentages of AMYF precursors (PDGFRα$^+$/α-SMA$^-$ cells) increased in X^-/Y mice compared with X/Y littermates at P2 and P6, suggesting the prevention of AMYF differentiation in X^-/Y mice. In contrast,

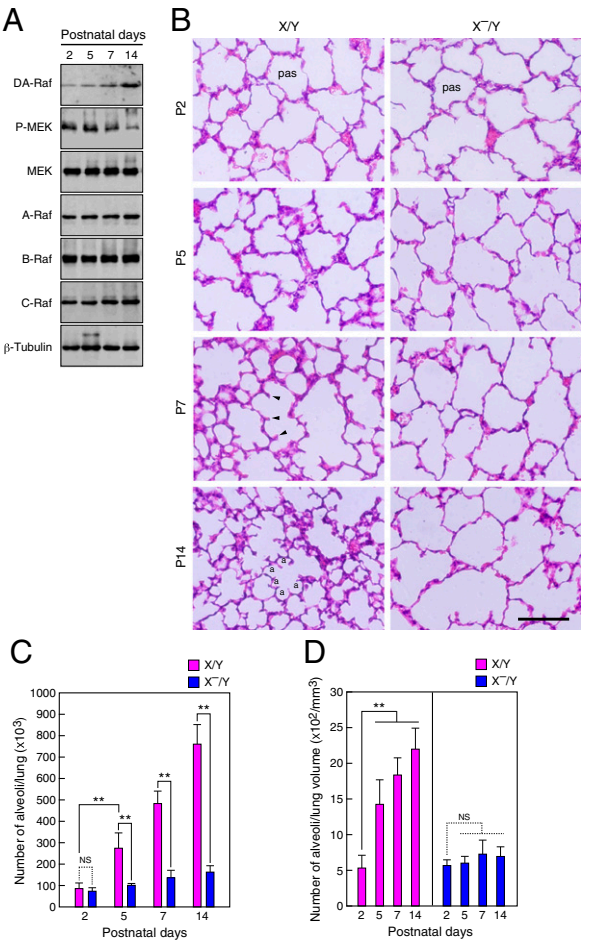

Fig. 1. DA-Raf–deficient mice have defective alveolar formation. (*A*) The protein levels of DA-Raf, Raf family members, and phosphorylated MEK1/2 in developing lungs from WT C57BL/6 mice were analyzed by Western blotting. (*B*) Sections from lungs at the indicated postnatal days of X/Y and X^-/Y mice were stained with H&E. Subdivision of prealveolar saccules (pas) by alveolar septa (arrowheads) at P7 results in the generation of alveoli (a) at P14 in X/Y mice. (Scale bar, 100 μm.) (*C* and *D*) The number of alveoli per lung (*C*) or per unit lung volume (*D*) in X/Y (pink bars) and X^-/Y (blue bars) mice was examined as described in *Materials and Methods* at the noted postnatal stages. The values represent means ± SD of three independent mice per genotype. $^{**}P < 0.01$; NS, $P > 0.05$.

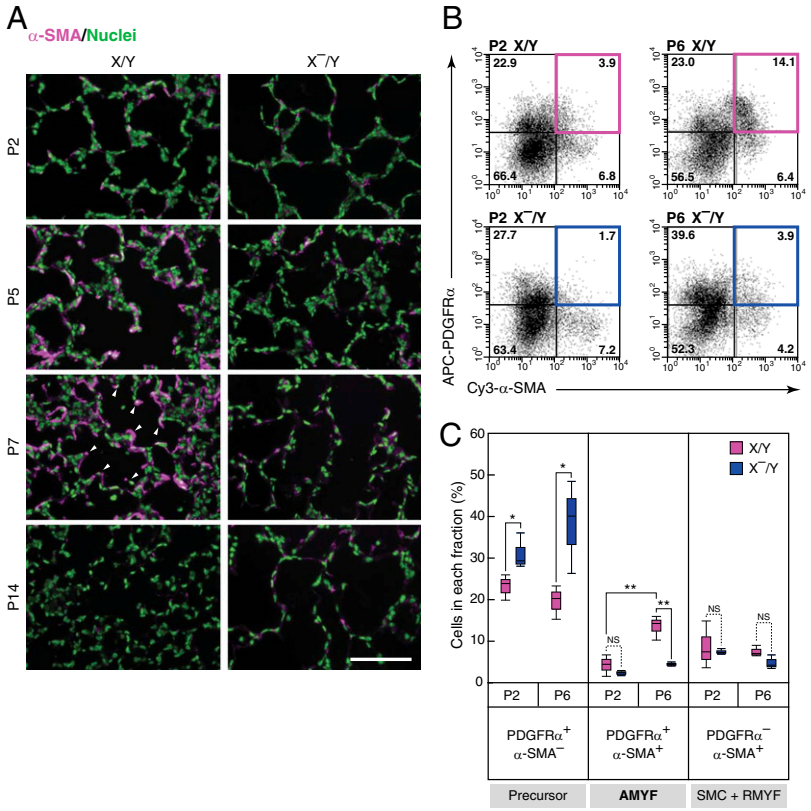

Fig. 2. Differentiation of AMYFs is blocked during alveolar formation in DA-Raf–deficient mice. (*A*) AMYFs expressing α-SMA (magenta) were examined by immunohistochemistry in lungs isolated from X/Y and X$^-$/Y mice at various postnatal ages. Arrowheads indicate the tips of alveolar septa. Nuclei are stained with Hoechst dye (green). (Scale bar, 100 μm.) (*B*) AMYFs expressing PDGFRα and α-SMA were determined by flow cytometric analysis by using the cell suspensions isolated from X/Y (*Upper*) and X$^-$/Y (*Lower*) lungs at P2 (*Left*) and P6 (*Right*). The *x* axis and *y* axis represent Cy3-α-SMA and APC-PDGFRα fluorescent intensities, respectively. The colored boxes show AMYF fractions. (*C*) Percentages of each quadrant in three independent mice per experimental groups are summarized. The fractions of AMYF precursor, AMYF, and SMC+RMYF contain PDGFRα$^+$/α-SMA$^-$ cells, PDGFRα$^+$/α-SMA$^+$ cells, and PDGFRα$^-$/α-SMA$^+$ cells, respectively. $^{**}P < 0.01$, $^{*}P < 0.05$; NS, $P > 0.05$.

the percentages of SMCs and RMYFs (PDGFRα$^-$/α-SMA$^+$ cells) in X$^-$/Y mice were comparable to those of X/Y mice. Although the amounts of mRNAs specific for myofibroblasts (*Acta2* and *Col1a1*) and α-SMA in X$^-$/Y mice were significantly less than those in X/Y littermates (Fig. S3 *C* and *D*), there were no differences in the amounts of mRNAs specifically expressed in AEC1s (*Pdpn* and *Aqp5*), AEC2s (*Sftpc1* and *Muc1*), and endothelial cells (*Pecam1* and *Cdh5*) between X$^-$/Y and X/Y lungs. In addition, staining for specific markers of AEC1s, AEC2s, and endothelial cells in the lungs was comparable between X/Y and X$^-$/Y mice (Fig. S3*E*). Thus, differentiation of AMYFs is specifically blocked in the lungs of X$^-$/Y mice.

DA-Raf Is Mainly Expressed in AEC2s That Are Distinct from AMYF Precursors. To clarify the mechanisms of defective AMYF differentiation in DA-Raf–deficient mice, we determined the cells expressing *DAraf* mRNA in developing lungs by in situ hybridization assay. Expression of *DAraf* mRNA was detected in round parenchymal cells located at alveolar corners at P7, and the expression level increased at P14 (Fig. 3*A*) consistently between AEC2s and *DAraf*-expressing cells. We further examined the expression of DA-Raf in AEC2s and AMYFs isolated from lungs by Western blotting. DA-Raf was highly expressed in AEC2s but only slightly expressed in the AMYF fraction (Fig. 3*B*). Furthermore, protein amounts of DA-Raf markedly increased in the isolated AEC2s from P2 to P14 (Fig. S4*A*), suggesting a distinct role of DA-Raf in AEC2s. Indeed, AEC2s also expressed other Raf family proteins (Fig. 3*B* and Fig. S4 *A* and *B*). These results imply that DA-Raf functions as a physiological inhibitor of Raf kinases in AEC2s during alveolar formation.

It is believed that some AMYFs develop from AEC2s through epithelial–mesenchymal transition in pulmonary fibrosis (21–23). Therefore, we predicted that AEC2s also give rise to AMYFs in developing lungs. To confirm this hypothesis, we crossed knock-in mice containing an internal ribosome entry site-CreERT2 cassette under the AEC2-specific (SP-C) promoter (24) to knock-in mice containing a floxed-STOP cassette with the *LacZ* gene at the ROSA26 locus (25) (Fig. 3*C*). To label AEC2s with LacZ for lineage tracing, 4-hydroxytamoxifen (4-OHT) was administered to pups after birth and at P1. All LacZ$^+$ cells were proSP-C$^+$ cells in lungs at P3 (Fig. S4*C*), confirming that AEC2s were correctly lineage labeled. However, lineage-labeled AMYFs (α-SMA$^+$/LacZ$^+$ cells) were scarcely found in the lungs at P5 by immunohistochemistry (Fig. 3*D*). Meanwhile, most lineage-labeled cells were α-SMA$^-$ (Fig. 3*E* and Fig. S4 *D* and *E*), indicating that AEC2s rarely differentiate into AMYFs at least in developing lungs. Moreover, very few proliferating AEC2s were detected in the lungs of X/Y and X$^-$/Y mice at P5, and number of AEC2s was comparable between X/Y and X$^-$/Y lungs (Fig. S4 *F* and *G*). These results suggest that it is unlikely that AMYFs are derived from AEC2s during alveolar formation.

DA-Raf Controls AMYF Differentiation Non–Cell-Autonomously. The results presented so far suggested that DA-Raf in AEC2s non–cell-autonomously regulates AMYF differentiation during alveolar formation. However, small amount of DA-Raf was detected

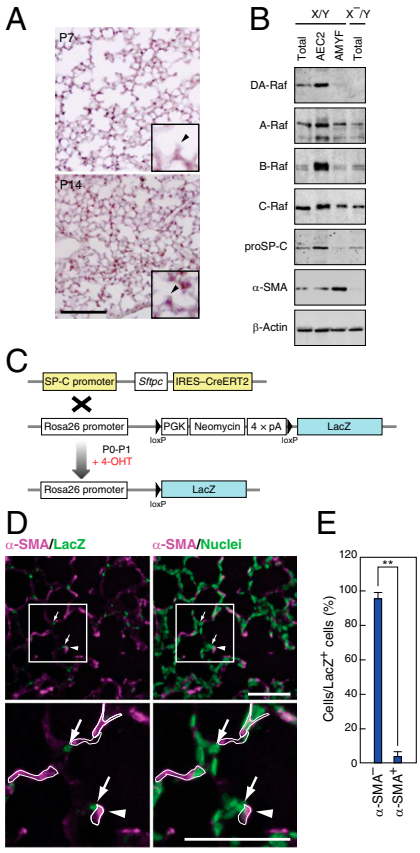

Fig. 3. DA-Raf is mainly expressed in AEC2s that are distinct from AMYF precursors. (*A*) *DAraf* mRNA was analyzed by in situ hybridization with a probe targeting the 3′ UTR of *DAraf* mRNA in lung sections from X/Y mice at P7 (*Upper*) and P14 (*Lower*). Enlarged images containing alveolar corners and alveolar septa (arrowheads) are shown in the inset of both images. (Scale bar, 100 μm.) (*B*) Lysates of total lungs, AEC2s, and AMYFs were isolated from X/Y or X^{-}/Y mice at P5 as described in *Materials and Methods*. These lysates were subjected to Western blotting to analyze the protein levels of DA-Raf and Raf family members. The markers for each fraction were analyzed with anti–proSP-C and anti–α-SMA. (*C*) Schematic representation of the strategy for lineage-trace of AEC2s. 4-OHT was subcutaneously injected into the pups generated from the crossing SP-C-CreERT2 knock-in mice with ROSA26-LacZ mice at P0 and P1. In the presence of 4-OHT, CreERT2 expressed in AEC2s translocates into the nucleus and mediates excision of the loxP-flanked neomycin cassette, which results in LacZ labeling of AEC2s. (*D*) Lineage-traced lungs were analyzed by staining for α-SMA and LacZ (*Left*) at P5. The same slide was stained with Hoechst dye (green) to visualize the nucleus of each cell (*Right*). *Lower* panels show higher-magnification images of enclosed squares in *Upper* panels. The borders of α-SMA^{+} cells are shown in white lines in *Lower* panels. Arrows and arrowheads indicate the lineage-labeled cells and alveolar septa, respectively. (Scale bar, 100 μm.) (*E*) Average percentages of α-SMA^{+} or α-SMA^{-} cells per lineage-labeled cells were determined in lungs from P5 mice. The values represent means ± SD of different 50 labeled cells from three independent individuals. (**$P < 0.01$).

in AMYFs (Fig. 3*B*); thus, we could not exclude the possibility that DA-Raf regulates AMYF differentiation cell-autonomously. To investigate the possibility, we took advantage of X-linked GFP transgenic mice. Because the *DAraf* gene is located on the X-chromosome, we used transgenic mice possessing the *GFP* transgene on the X chromosome (X^{GFP}) to monitor X-inactivation (26–28). X^{-}/X females were crossed with X^{GFP}/Y males to generate X^{GFP}/X^{-} females (Fig. 4*A*). Real-time PCR analysis showed significant reduction of *DAraf* mRNA in GFP^{-} (inactive-X^{GFP}) lung cells, but an equivalent level in GFP^{+} (active-X^{GFP}) cells in lung cells from X^{GFP}/X^{-} females compared with that of X^{GFP}/X mice (Fig. 4*B*). If DA-Raf regulates AMYF differentiation cell-autonomously, GFP^{+} (i.e., DA-Raf–expressing) cells but not GFP^{-} cells differentiate into AMYFs in X^{GFP}/X^{-} mice (Fig. 4*C*). However, not only the percentage of α-SMA^{+} cells within GFP^{-} lung cells but also that within the GFP^{+} population were dramatically reduced in X^{GFP}/X^{-} mice compared with X^{GFP}/X mice (Fig. 4*D*). When the percentages of α-SMA^{+} cells within GFP^{+} lung cells were compared with those within GFP^{-} cells, both percentages were similar (around 25%) in X^{GFP}/X mice (Fig. 4*E*), indicating that GFP expression did not affect on AMYF differentiation. Both percentages of α-SMA^{+} cells within GFP^{+} or GFP^{-} lung cells from X^{GFP}/X^{-} mice were similar (around 10%) and significantly lower than those of X^{GFP}/X mice. Therefore, these data indicate that DA-Raf regulates AMYF differentiation in a non–cell-autonomous manner. In addition, there were no significant differences in the percentages of α-SMA^{+} cells between X^{GFP}/X^{-} and X^{-}/Y mice, suggesting a suppressive effect of GFP^{-} (DA-Raf–nonexpressing) cells on the differentiation of AMYFs. To explore whether this effect of DA-Raf–nonexpressing cells is local or systemic, we further examined the spatial pattern of AMYFs in lungs of X^{GFP}/X^{-} mice. There were insular clumps of GFP^{+} and GFP^{-} cells in one lobe of X^{GFP}/X^{-} lungs, and the GFP-high area contained many AMYFs compared with the GFP-low area (Fig. 4*F*). Indeed, the intensity of α-SMA expression in 150-μm square alveolar fields of X^{GFP}/X^{-} lungs was highly correlated with that of GFP expression in the same fields ($r = 0.79$, $P < 0.01$) (Fig. 4*G*). In addition, the percentages of α-SMA^{+} cells in lungs of X^{GFP}/X^{-} and X^{-}/Y mice were strikingly decreased independent of body weights, which excluded a systemic effect of DA-Raf on AMYF differentiation (Fig. S5*A*). These results suggest that DA-Raf regulates the local alveolar environment to induce AMYF differentiation. As a result, lungs of X^{-}/X mice at P14 contained insular clumps of small and large alveoli (Fig. S5*B*). Taken together, these findings suggest that *DAraf*-inactivated cells prevent surrounding cells from differentiating into AMYFs in lungs of X^{-}/X mice (Fig. 4*H*).

DA-Raf–Dependent Inactivation of MEK1/2 in AEC2 Promotes AMYF Differentiation During Alveolar Formation. Because DA-Raf negatively regulates the level and duration of MEK1/2 activity in mouse embryonic fibroblasts (Fig. S6 *A* and *B*), we examined the effects of DA-Raf on the Ras-ERK signaling pathway by analyzing MEK1/2 activity at various time points during alveolar formation. Immunohistochemical analysis for phosphorylated MEK1/2 demonstrated a substantial activation of MEK1/2 in a portion of proSP-C^{+} cells in both X/Y and X^{-}/Y mice, but not in α-SMA^{+} cells in X/Y mice at P5 (Fig. 5*A* and Fig. S6*C*). Although the cells containing highly phosphorylated MEK1/2 decreased in the lungs of both X/Y and X^{-}/Y mice from P2 to P14, the percentages of these cells in lungs of X^{-}/Y mice were higher than those of X/Y mice from P2 to P7, but not at P14 (Fig. 5*B*). These results suggest the physiological requirement of DA-Raf for inactivation of MEK1/2 in AEC2s during alveolar formation.

We further examined whether augmented phosphorylation of MEK1/2 was responsible for defective AMYF differentiation in lungs of X^{-}/Y mice by using an inhibitor of MEK1/2 (MEKi), PD0325901, in vivo. The effective-dose of the MEKi (Fig. S6*D*) was administered to X^{-}/Y mice from P1 to P5, and AMYFs were analyzed at P6 by flow cytometry. The MEKi clearly restored the percentage of AMYF fraction in X^{-}/Y mice (Fig. 5*C*). Furthermore, the percentages of the fractions containing AMYF precursors in X^{-}/Y mice injected with MEKi recovered to a normal level, but the fractions of SMCs and RMYFs remained constant (Fig. 5*D*). Collectively, these results suggest that augmentation of phosphorylated MEK1/2 in AEC2s of X^{-}/Y mice negatively regulates AMYF differentiation during alveolar formation.

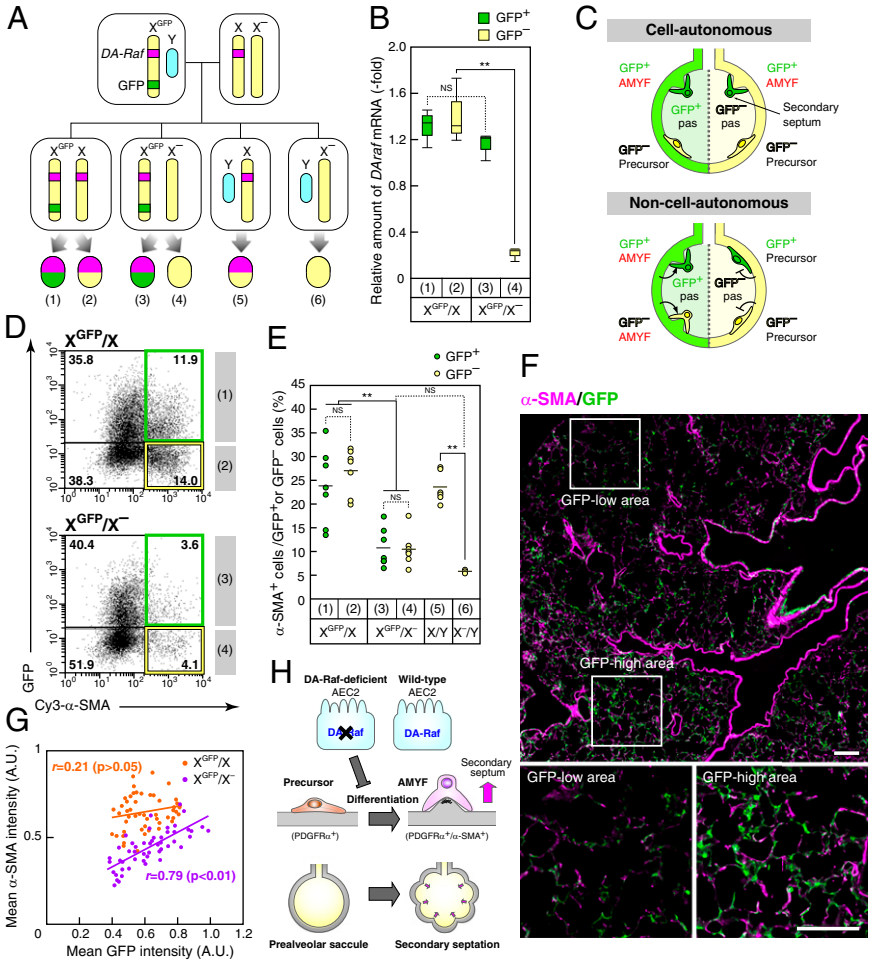

Fig. 4. DA-Raf controls AMYF differentiation non–cell-autonomously. (*A*) Breeding scheme for generating X^{GFP}/X^{-} mice. Interbreeding of X^{-}/X mice to X^{GFP}/Y males results in X^{GFP}/X^{-} mice, which are comprised of GFP^{+} (active-X^{GFP} and DA-Raf–expressing) cells (3) and GFP^{-} (inactive-X^{GFP} and DA-Raf–nonexpressing) cells (4). X^{GFP}/X mice, which contain intact GFP^{+} (1) and GFP^{-} cells (2), were used as sex-matched controls. The cells with no fluorescence from X/Y (5) and X^{-}/Y mice (6) were also used as controls. (*B*) Lung cell suspensions were isolated from lungs X^{GFP}/X^{-} and X^{GFP}/X mice at P5 and sorted based on GFP expression by FACS. The box plot represents relative amounts of *DAraf* mRNA in each fraction of three independent mice per genotype. $^{**}P < 0.01$; NS, $P > 0.05$. (*C*) Schematic representation of the analysis with X^{GFP}/X^{-} mice. If DA-Raf acts cell-autonomously, GFP^{+} cells behave normally, and GFP^{-} cells do not differentiate into AMYFs, similar to DA-Raf–deficient mice. Conversely, if DA-Raf functions non–cell-autonomously, the cells equally differentiate into AMYFs within their surrounding stimuli independent of GFP expression. (*D*) Representative FACS dot plots of the lung cell suspensions from X^{GFP}/X (*Upper*) and X^{GFP}/X^{-} (*Lower*) mice are shown. The *x* axis and *y* axis represent Cy3-α-SMA and GFP fluorescent intensities, respectively. (*E*) Average percentages of $\alpha\text{-SMA}^{+}$ cells within the GFP^{+} (green circles) or GFP^{-} (yellow circles) cells in X^{GFP}/X, X^{GFP}/X^{-}, X/Y, and X^{-}/Y are summarized. The circles indicate values from individual mice, and lines indicate medians in each group. $^{**}P < 0.0$; NS, $P > 0.05$. (*F*) Sections from lungs of X^{GFP}/X^{-} mice at P5 were stained for α-SMA (magenta) and GFP (green). *Lower* panels show the higher-magnification images of the enclosed white squares in the *Upper* panel. (Scale bar, 100 μm.) (*G*) Fluorescence intensities of α-SMA and GFP in small alveolar areas (150-μm squares) from X^{GFP}/X (orange circles) and X^{GFP}/X^{-} (purple circles) mice were analyzed as described in *Materials and Methods*. The lines show linear regression. *r* and *P* values indicate Pearson's correlation coefficients and probability, respectively. (*H*) Proposed model for non–cell-autonomous regulation of AMYF differentiation by DA-Raf in AEC2s.

DA-Raf–Dependent Inactivation of MEK1/2 Suppresses TIMP4 Expression and Induces a Subsequent Proteolytic Cascade MMP14–MMP2. To identify negative and local secretory factors produced by AEC2s of X^{-}/Y mice, we performed cDNA microarray analysis. Genes with more than a twofold change in expression levels in X^{-}/Y mice compared with X/Y littermates were selected as candidates (Dataset S1). Among these genes, we focused on *Timp4*, which codes for a protein acting as an endogenous inhibitor of metalloproteinases including MMP14 and MMP2 (29, 30). By real-time PCR analysis, we confirmed that *Timp4* expression in total lungs and AEC2s of X^{-}/Y mice was increased compared with those of X/Y littermates (Fig. 6*A*). Furthermore, *Timp4* expression was significantly concentrated in AEC2s of X^{-}/Y mice in comparison with total lungs of X^{-}/Y mice (Fig. 6*A* and Fig. S7*A*). Immunohistochemical analysis in P5 mice also showed extensive expression of TIMP4 in proSP-C^{+} cells in X^{-}/Y mice (Fig. S7*B*). Because TIMP4 suppresses MMP14 and intermediate-MMP2, which are involved in the process of MMP2 activation (31, 32), we further examined the amount of activated MMP2 in lungs of X^{-}/Y mice. Gelatin zymography with lung extracts at P5 showed that the amount of activated MMP2 but not MMP9 was decreased in lungs of X^{-}/Y mice (Fig. 6*B* and Fig. S7*C*). Indeed, the activity of an immunoprecipitated MMP14 from lung lysates of X^{-}/Y mice decreased compared with that of X/Y mice at P5 (Fig. 6*C*). In contrast, expression levels of *Mmp2*, *Mmp9*, and *Mmp14* mRNA in lungs of X^{-}/Y mice were similar to those of X/Y littermates (Fig. 6*D*). These results suggest that enhanced expression of *Timp4* in AEC2s regulates MMP14–MMP2 proteolytic cascade in X^{-}/Y lungs. During alveolar formation, levels of activated MMP2 were inversely correlated to those of

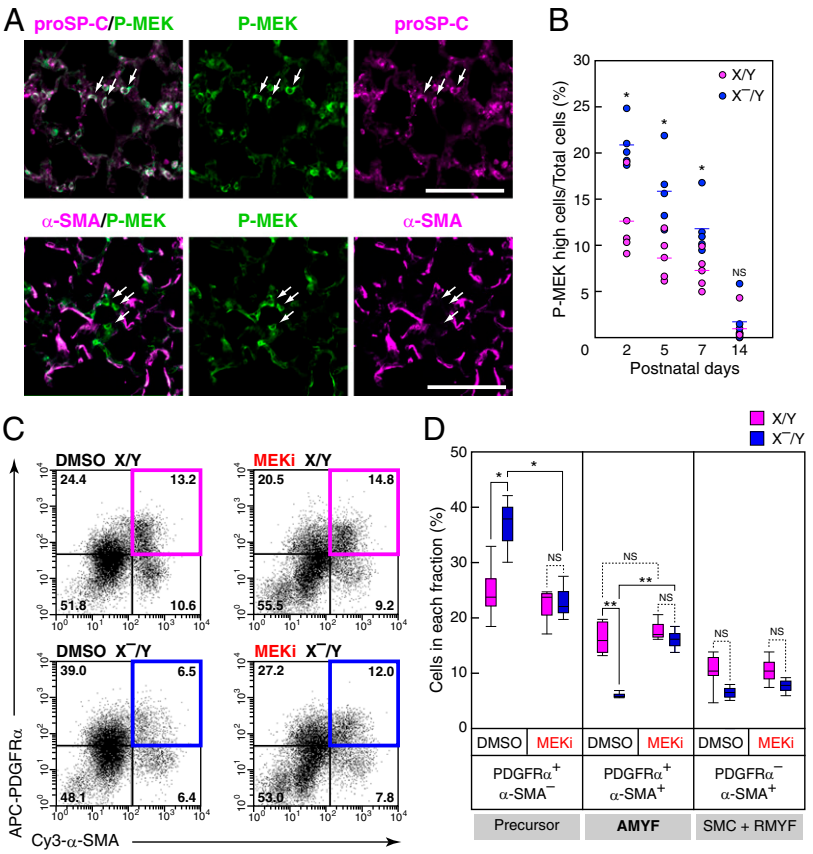

Fig. 5. DA-Raf–dependent inactivation of MEK1/2 in AEC2 promotes AMYF differentiation during alveolar formation. (*A*) Distribution of phosphorylated MEK1/2 (P-MEK) was analyzed in lungs of X/Y mice at P5 by immunohistochemistry. Double-immunofluorescence staining for P-MEK (green) and proSP-C (*Upper*) or α-SMA (*Lower*) was performed. Arrows indicate representative cells with high P-MEK levels. (Scale bar, 100 μm.) (*B*) The percentages of cells containing high levels of P-MEK in lungs of X/Y (pink circles) and X^{-}/Y (blue circles) mice were analyzed at the indicated postnatal ages, as described in *Materials and Methods*. Circles and lines indicate individual mice and median values, respectively. *$P < 0.05$; NS, $P > 0.05$. (*C*) Representative FACS dot plots of the lung cell suspensions from X/Y (*Upper*) and X^{-}/Y (*Lower*) mice treated with DMSO (*Left*) and MEKi, PD0325901, (*Right*). The *x* axis and *y* axis represent Cy3-α-SMA and APC-PDGFRα fluorescent intensities, respectively. (*D*) Percentages of each quadrant in four independent mice per experimental groups are summarized. The fractions of AMYF precursor, AMYF, and SMC+RMYF contain PDGFRα^{+}/α-SMA^{-} cells, PDGFRα^{+}/α-SMA^{+} cells, and PDGFRα^{-}/α-SMA^{+} cells, respectively. **$P < 0.01$, *$P < 0.05$; NS, $P > 0.05$.

TIMP4 and DA-Raf expression in WT C57BL/6 mice (Fig. 6*E* and Figs. S4*A* and S7*D*), suggesting a temporal relationship among these molecules. In addition, there was a weak inverse correlation ($r = -0.56$, $P < 0.01$) between the intensities of TIMP4 and those of GFP in lungs of X^{GFP}/X^{-} mice at P5 (Fig. S7*E*), supporting a spatial link between TIMP4 and DA-Raf. To determine signaling pathway leading to increased *Timp4* expression in X^{-}/Y mice, MEKi was administered into mice from P1 to P5. Both mRNA and protein levels of *Timp4* were restored to the control levels in X^{-}/Y mice following inhibitor treatment (Fig. 6 *F* and *G* and Fig. S7*F*). Furthermore, impaired MMP2 activity in X^{-}/Y lungs was recovered to the control level by the treatment of MEKi (Fig. 6*H* and Fig. S7*G*). These results suggest that DA-Raf–dependent inhibition of MEK1/2 activity suppresses TIMP4 expression, which promotes a subsequent proteolytic cascade MMP14–MMP2 during alveolar formation.

MMP14–MMP2 Proteolytic Cascade Regulates AMYF Differentiation During Alveolar Formation. MMP2-deficient mice exhibit abnormal saccular development, and similar phenotypes are found in epidermal growth factor receptor (EGFR)-deficient mice in which MMP14 expression is extensively impaired (10, 12). Thus, we next examined whether MMP14–MMP2 proteolytic cascade was required for AMYF differentiation during postnatal alveolar formation. First, to determine the contribution of MMP2 to alveolar formation, the activity of general MMPs was measured by using an inhibitor of MMP2 (MMPi), MMP2 inhibitor III, in the lung extracts at P5 (Fig. S8*A*). The generic MMP activity in lungs was decreased to an equivalent level in X^{-}/Y mice by the addition of this inhibitor, implying the possibility of off-target effects on other MMPs. Thus, we further analyzed the activities of MMP14 and MMP9, which have the highest possibility to be inhibited by MMPi (33). This inhibitor of MMP2 markedly suppressed the activity of MMP14 as well as MMP2, but not MMP9 (Fig. S8 *B–D*); thus, we used that as an inhibitor of MMP14 and MMP2. Therefore, to define the role of MMP14–MMP2 proteolytic cascade, MMPi was administered to WT mice from P1 to P6, and then lung cells at P6 were analyzed by flow cytometry. The percentage of the AMYF fraction decreased by MMPi (Fig. 7*A*). However, MMPi increased the percentages of the precursor fractions but did not alter that of the SMC and RMYF fractions (Fig. 7*B*). In addition to the abrogation of AMYF differentiation (Fig. S8*E*), interference with alveolar formation represented by the enlarged alveolar occurred in the lungs of inhibitor-treated mice (Fig. 7*C*). Although lung volumes were comparable between the groups, the number of alveoli was significantly decreased by inhibitor treatment (Fig. 7 *D* and *E*). These results indicate that MMP14–MMP2 proteolytic cascade

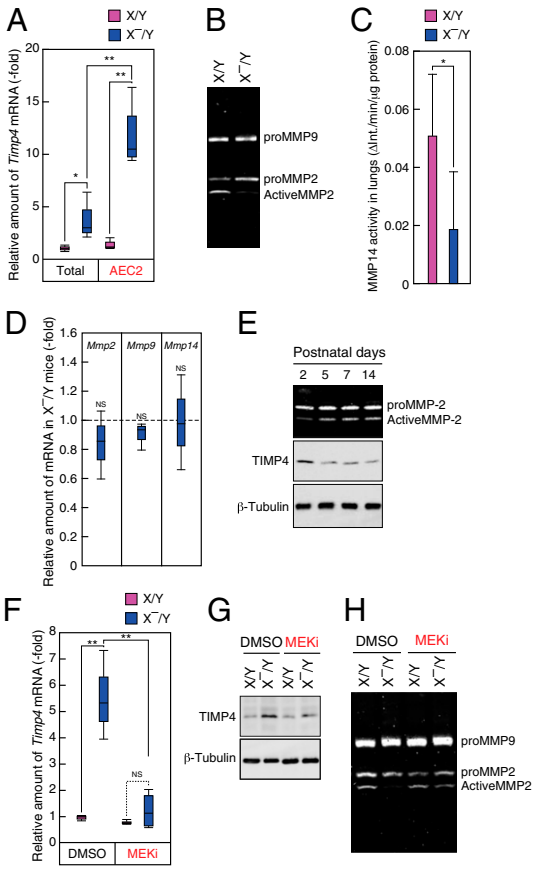

Fig. 6. DA-Raf-dependent inactivation of MEK1/2 suppresses TIMP4 expression and induces a subsequent proteolytic cascade MMP14–MMP2. (*A*) Total lungs and AEC2s were collected from X/Y (pink boxes) and X⁻/Y (blue boxes) mice at P5, and the expression levels of *Timp4* were analyzed by using real-time PCR. (*B*) Lung lysates isolated from X/Y and X⁻/Y mice were subjected to the gelatin zymography analysis. (*C*) Activity levels of MMP14 in the lungs of X/Y (pink bar) and X⁻/Y (blue bar) mice at P5 were analyzed by FRET-based assay as described in *SI Materials and Methods*. The values represent means ± SD. (*D*) The expression levels of *Mmp2*, *Mmp9*, and *Mmp14* in lungs at P5 from X/Y and X⁻/Y mice were analyzed by real-time PCR. Values represent the amounts of mRNA relative to those in WT littermates, which are arbitrarily defined as 1. (*E*) MMP2 activity (*Top*) was analyzed by zymography using lysates from developing lungs. The amounts of TIMP4 (*Middle*) and β-Tubulin (*Bottom*) were examined by Western blot analysis at indicated postnatal ages. (*F* and *G*) The expression levels of *Timp4* in lungs at P6 from X/Y and X⁻/Y mice treated with DMSO or MEKi were examined by using real-time PCR (*F*) or Western blot analysis (*G*). (*H*) MMP2 activity levels were analyzed gelatin zymography by use of lung lysates isolated from X/Y and X⁻/Y mice treated with DMSO or the MEKi. In *A*, *C*, *D*, and *F* the analyses were performed with three to five independent mice per genotype. $^{**}P < 0.01$, $^{*}P < 0.05$; NS, $P > 0.05$.

plays an essential role in AMYF-mediated secondary septation during alveolar formation.

To examine whether the DA-Raf–regulated signaling pathway is required for pulmonary function, we measured oxygen saturation in X/X and X⁻/X mice by pulse oximetry after exercise. Although X⁻/X mice showed normal blood-oxygen saturation before exercise, reductions of blood-oxygen levels were detected in X⁻/X mice after exercise compared with X/X mice (Fig. S8*F*). This result suggests that DA-Raf–mediated alveolar formation is critical for the normal pulmonary function.

In conclusion, the enhanced activity of MEK1/2 in DA-Raf–deficient AEC2s leads to the expression of TIMP4, which suppresses a subsequent proteolytic cascade MMP14–MMP2. Finally, the activation of MMP2 induces differentiation from AMYF precursors into AMYFs followed by the secondary septation during alveolar formation (Fig. 7*F*).

Discussion

Through the analysis of DA-Raf–deficient mice, our study clarifies the role of the Ras-ERK signaling pathway in alveolar formation. In fetal lung, the fibroblast growth factor 10 (FGF10) -activated Ras-ERK signaling pathway is essential for tracheal branching. During tracheal morphogenesis, the distribution of the activated ERK1/2 in epithelial cells at terminal lung buds is regulated by Sprouty1/2, which determines mitotic spindle orientation and airway shape (14, 15). Furthermore, the Ras-ERK signaling pathway in $Sox9^{+}$ cells at the branch tips of developing lungs regulates the balance between branching and alveolar differentiation (16). Our findings demonstrate that DA-Raf predominantly inhibits the Ras-ERK signaling pathway in AEC2s during alveolar formation. Collectively, these data show that the spatiotemporally regulated Ras-ERK signaling pathway is one of the most important key regulators for both fetal and postnatal development of lungs.

It has been known that the magnitude, duration, and subcellular localization of ERK1/2 determine distinct cellular responses in a cell-type–specific manner (34). In the present study, the phosphorylation levels of MEK1/2 in AEC2s gradually declined along with the progression of alveolar formation in WT mice, implying the physiological significance of the activation patterns of the Ras-ERK signaling pathway in AEC2s. The detailed analysis of MEK1/2 and ERK1/2 activation in DA-Raf–deficient mouse embryonic fibroblasts reveals that DA-Raf can regulate the magnitude and duration of the Ras-ERK signaling pathway upstream of MEK1/2. Furthermore, prolonged MEK1/2 activation in DA-Raf–deficient AEC2s was detected until P7 during alveolar formation. Therefore, DA-Raf appears to physiologically determine cellular responses by regulating the activation patterns of the Ras-ERK signaling pathway in AEC2s. Because all Raf family members were expressed in AEC2s, and none of the genetic studies has provided their relevance to alveolar formation (35–39), phenotypic analyses in AEC2-specific knockout mice lacking each member will be needed.

Our analysis resolved a longstanding question about how AMYF precursors differentiate into AMYFs during alveolar formation. Because PDGF-A–deficient mice lack AMYFs and AMYF precursors expressing PDGFRα in the alveolar region, it has been suggested that these cells migrate from proximal to peripheral area of lungs in response to epithelial-derived PDGF-A during alveolar formation (3, 4). Although AMYF precursors were comparable between WT and DA-Raf–deficient mice at P2, these cells increased in DA-Raf–deficient mice at P6 because of impaired AMYF differentiation, implying that PDGF-A/PDGFRα signaling pathway is normally activated in DA-Raf–deficient mice. These results clearly suggest that other mechanisms underlie AMYF differentiation in addition to the migration of AMYF precursors mediated by the PDGF-A/PDGFRα signaling pathway. In the present study, we show that DA-Raf in AEC2s regulates AMYF differentiation in a non–cell-autonomous manner, which highlights the importance of the AEC2–AMYF precursor interaction in alveolar formation. Accordingly, similar to other types of organogenesis, the epithelial–mesenchymal interaction is one of the critical factors for alveolar formation. Collectively, these data show that AMYF is induced by two steps, migration of AMYF precursors to the peripheral area of lungs and AEC2-induced AMYF differentiation, which might determine the precise localization of the secondary septa.

We identified TIMP4 as a local inhibitory factor secreted from DA-Raf–deficient AEC2s. Previously, the activated MEK1/2-mediated transcriptional control of *Timp4* has been implicated in chondrocytes (40). In addition, aberrant *Timp4* expression has been identified in cancer (29), and the mouse *Timp4* promoter contains potential binding sites for Ets family members, which

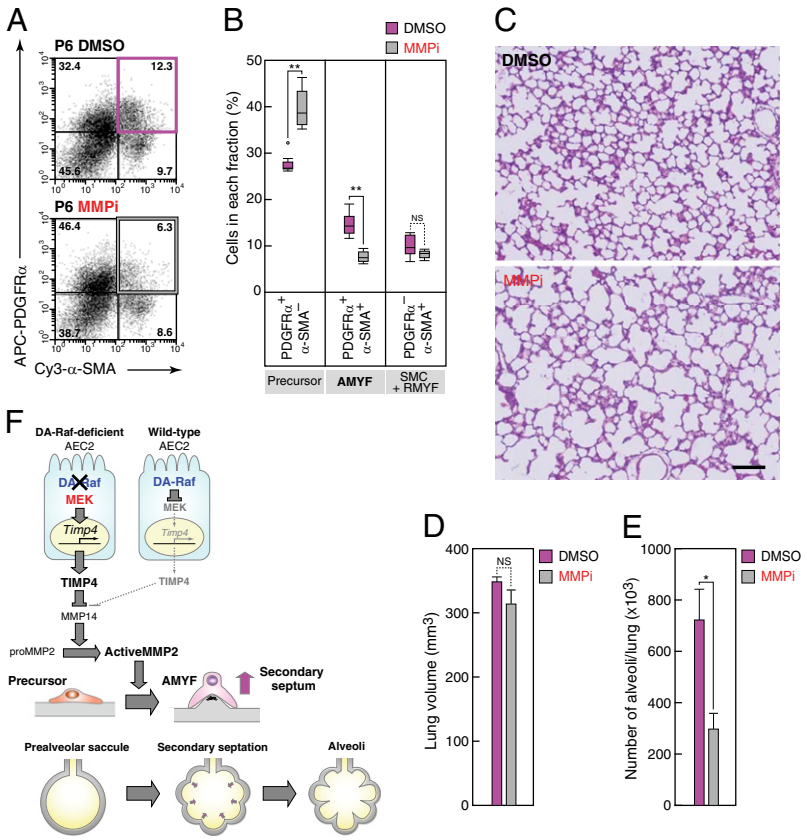

Fig. 7. MMP14-MMP2 proteolytic cascade regulates AMYF differentiation during alveolar formation. (*A*) Representative FACS dot plots of lung cell suspensions from WT C57/BL6 mice treated with DMSO (*Upper*) or MMPi (*Lower*), an inhibitor of MMP2 and MMP14. The *x* axis and *y* axis represent Cy3-α-SMA and APC-PDGFRα fluorescent intensity, respectively. The colored boxes show AMYF fractions. (*B*) Percentages of each quadrant of three independent mice per treatment are summarized. The fractions of AMYF precursor, AMYF, and SMC+RMYF contain PDGFRα$^+$/α-SMA$^-$ cells, PDGFRα$^+$/α-SMA$^+$ cells, and PDGFRα$^-$/α-SMA$^+$ cells, respectively. (*C*) Sections were obtained from the lungs of P14 mice continuously treated with DMSO (*Upper*) or MMPi (*Lower*) from P1 to P14 and then stained with H&E. (Scale bar, 100 μm.) (*D* and *E*) The lung volumes (*D*) and alveolar numbers (*E*) per total lungs in P14 mice with (gray bars) or without (pink bars) MMPi were examined as described in *Materials and Methods*. The values represent means ± SD. In *B*, *D*, and *E* the analyses were performed with three to five independent mice per genotype. $^{**}P < 0.01$, $^{*}P < 0.05$; NS, $P > 0.05$. (*F*) A model illustrating the non–cell-autonomous role of DA-Raf in AMYF differentiation during alveolar formation. Ablation of DA-Raf in mice leads to augmented phosphorylation of MEK1/2 in AEC2s and non–cell-autonomously prevents AMYF differentiation. TIMP4 produced by DA-Raf–deficient AEC2s leads to inactivation of MMP14–MMP2 signaling pathway, which is required for AMYF differentiation and the secondary septation in developing lungs.

are transcription factors activated by the Ras-ERK signaling pathway (41). These findings imply the involvement of the Ras-ERK signaling pathway in transcriptional control of *Timp4*. Consistent with overexpression of *Timp4*, MMP2 and MMP14 activities in the lungs of DA-Raf–deficient mice were significantly lower than those in WT mice. Previous studies have demonstrated that mice lacking MMP2 or MMP14 exhibit severe airspace enlargement and pulmonary hypoplasia (10–12). In accordance with a substantial contribution of MMP14 and MMP2 to generic MMPs activity at P5, continuous treatment of WT mice with MMPi abrogated the differentiation of AMYFs and the secondary septation, to a lesser extent, similar to that found in DA-Raf–deficient mice. Therefore, impaired MMP14 and MMP2 activities partly account for the defective alveolar formation in DA-Raf–deficient mice.

In the present study, we could not identify the proteolytic targets of MMP2 during alveolar formation. Latent TGF-β1 might be a substrate for MMP2. TGF-β1 induces α-SMA expression and differentiation into myofibroblast from pulmonary fibroblast including PDGFRα$^+$ cells in vitro (5). In addition, MMP-2 proteolytically cleaves and activates latent TGF-β1 (42). Furthermore, the mice lacking the component of latent TGF-β1 complex represent defective alveolar formation (43, 44). Taken together, these data show that AEC2-mediated balance between MMP2 and TIMP4 might determine the spatiotemporal availability of active TGF-β1 and underlie the AMYF differentiation, but it remains to be elucidated. In addition, it has been shown that ECM proteins including elastin, collagen, and fibronectin, deposited by AMYFs, are substrates for MMP2 (45). Thus, MMP2-mediated ECM remodeling may coordinately contribute to AMYF-mediated morphological changes of alveolar walls in the secondary septation.

Our study demonstrates a novel link between the role of the Ras-ERK signaling pathway in AEC2s and AMYF differentiation in alveolar formation. Although the Ras-ERK signaling pathway in AEC2s seems to be highly related to AMYF differentiation, this relationship has only be shown in FGF receptor (FGFr) 3 and FGFr4 double-knockout mice. These *FGFr3* and *FGFr4* genes encode receptors for FGFs and are expressed in AEC2s, and double-knockout mice lacking these genes display excessive AMYFs (46, 47). In contrast, DA-Raf–deficient mice, which displayed augmented MEK1/2 activity in AEC2s, had significantly reduced AMYFs. Accordingly, there is an apparent inverse correlation between AMYF differentiation and the Ras-ERK signaling activity in AEC2s. Therefore, negative regulation of the Ras-ERK signaling pathway in AEC2s seems to act as a timer that triggers differentiation of AMYFs.

Regeneration of alveoli is an attractive therapeutic approach for COPD characterized by extensive destruction of alveolar

walls. After pneumonectomy, alveolar formation occurs along with the increase of lung volume (48, 49). Besides adding new alveolar units, AMYF-mediated secondary septation also occurs during pneumonectomy-induced compensatory lung growth at least in mouse model (13, 50). Therefore, adult lungs have the ability to reproduce developmental events in many mammalian species, including humans. In the present study, measurement of blood-oxygen saturation after exercise in adult DA-Raf heterozygous female mice revealed similarities to the symptoms of patient with COPD. Thus, we believe that new therapies for COPD by targeting for DA-Raf–mediated signaling pathways in AEC2s can be developed.

Materials and Methods

Morphometry. Lungs for morphometric analysis were fixed according to the method described previously (51). Whole lung volumes were estimated by the Cavalieri method. Sampling of lung tissue was conducted by use of tissue fractionator after embedding in 4% (wt/vol) Agar. Alveolar numbers were estimated by counting alveolar rings in serial sections using the values of parenchymal volumes calculated by point counting, as described previously (52, 53).

Tissue Preparation and Immunohistochemistry. After perfusion with PBS, the lungs were inflated and fixed with 4% (wt/vol) paraformaldehyde (PFA) in 0.1 M Na-PO_4 buffer (pH 7.4) through the trachea. Tissues were embedded in paraffin wax or infused with 30% (wt/vol) sucrose followed by freezing in Tissue-Tec OCT compound (Sakura). For histological examination, tissue sections were cut from paraffin-embedded blocks of lungs 4-μm thick and stained with H&E. The 4-μm-thick sections were cut from the frozen block and dried. If necessary, antigen retrieval was carried out, and sections were permeabilized with 0.1% TritonX-100 in PBS. After blocking with blocking buffer (1% BSA in 1×TBS), sections were immunostained with Cy3-conjugated anti–α-SMA, anti-GFP, anti-LacZ anti-phospho-MEK1/2, anti–proSP-C, and anti-TIMP4 antibody diluted in appropriate buffer, and then these antibodies were applied to the sections. Detection was carried out with fluorescent species-matched secondary antibody. The nuclei were stained with Hoechst 33258 (Life Technologies). The specimens were observed with Zeiss Axioskop microscope (Carl Zeiss). For staining with Cy3-conjugated anti–α-SMA mAb, rabbit anti-GFP pAb, and anti–proSP-C pAb, the sections were incubated with 1:200 dilutions of the antibodies in blocking buffer at room temperature for 1–2 h. For staining of LacZ, the sections were incubated with a 1:100 dilution of the antibody in blocking buffer for overnight at 4 °C. For detection of phospho-MEK1/2 and TIMP4, antigen retrieval was carried out by subjecting slides to microwave treatment in 0.01 M sodium citrate buffer (pH 6.0) and the sections were incubated with a 1:200 dilution of antiphospho-MEK1/2 pAb in SignalStain Antibody Diluent (Cell Signaling Technology) for overnight at 4 °C. For BrdU staining, paraffin-embedded lung sections were deparaffinized and subjected to antigen retrieval conducted by microwave for 15 min in 0.01 M sodium citrate buffer (pH 6.0). Then, the sections were incubated with anti-BrdU mAb diluted in blocking buffer 1:200 for 1 h at room temperature. After washing with PBS, the sections were incubated with 1:1,000 dilutions of A488- or A555-conjugated secondary antibodies for 1 h at room temperature. For quantitative analyses of GFP, α-SMA, TIMP4, and phospho-MEK1/2, microscopic images were further analyzed by ImageJ. For double-staining of lungs with the antibodies for phospho-MEK1/2 and proSP-C or TIMP4 and proSP-C, antibodies were labeled using Zenon labeling kit (Life Technologies), according to the manufacturer's protocol.

Preparation of Lung Cells. Suspension of lung cells was obtained according to modified protocol described previously (54). Briefly, lung was perfused with PBS and injected with 1 mg/mL collagenase (Sigma) in PBS thorough the trachea, then incubated for 20 min at 37 °C. Dissections were taken off lobes and minced into small pieces. To obtain a single-cell suspension, we used 50 μg/mL DNaseI and passed the cells through a cell strainer (Falcon). For FACS analysis, erythrocytes were eliminated by the incubation in lysis buffer (0.15 M NH_4Cl, 10 mM $KHCO_3$, 0.1 mM EDTA) for 2 min at room temperature. For FACS analysis, the cells were washed twice with PBS and then conducted staining. Isolation of AEC2s was performed according to modified protocols described previously (54, 55). Dispersed cells were centrifuged in a Percoll (GE Healthcare) density gradient (25–65% vol/vol), and second and third bands were taken out from a total of five fractions. The suspension of AEC2s was further purified by magnetic activated cell separation depletion of macrophage and leukocytes using APC-conjugated anti-CD11b mAb and APC-conjugated anti-CD45 mAb. Furthermore, adhesion-based negative selection was performed to eliminate fibroblasts. Pepstatin A (10 μg/mL) and MG132 (5 μM) were added in all steps of purification after digestion of lungs by collagenase, to inhibit lysosomal proteases and proteasome, respectively. For culture of lung fibroblasts, lungs were removed without the large airway from mice following perfusion with PBS and incubated 10 min in FBS-free DMEM at room temperature. Then, lungs were extensively minced into small pieces and cultured in DMEM containing 10% (vol/vol) FBS for 7 d at 37 °C. Medium was changed every 2 d.

FACS Analysis. For PFGFRα staining, the isolated cells were incubated with APC-conjugated anti-PDGFRα in PBS for 30 min on ice. For α-SMA staining, the cells were fixed with Foxp3 Fixation/Permeabilization product (eBioscience) according to the manufacturer's protocol before staining. After fixation, the cells were incubated with Cy3-conjugated anti–α-SMA in PBS containing 5% (vol/vol) FBS for 30 min at room temperature. After the extensive washing, the cells were analyzed by flow cytometer (BD Biosciences).

RNA Isolation and Quantitative PCR. Total RNA of lungs was purified using RNeasy Plus Kit (QIAGEN), and reverse transcription of mRNA was performed using the SuperScript VILO cDNA Synthesis Kit (Life Technologies) according to the manufacturer's protocol. Real-time PCR was performed on the 7300 Real-Time PCR system (Applied Biosystems) using the Power SYBR Green PCR Master Mix (Applied Biosystems) and specific primers. Primers used for real-time PCR are listed in *SI Materials and Methods*.

Western Blotting and Immunoprecipitation. Western blotting was carried out as described previously (56). For the analysis using antibodies for DA-Raf and phospho-proteins, antibodies were diluted with Can Get signal immunoreaction enhancer solution (TOYOBO) and applied to membranes for overnight at 4 °C. For immunoprecipitation assay, lungs were homogenized in lysis buffer containing 1% Nonidet P-40, 5% (vol/vol) glycerol, 50 mM Tris·HCl (pH7.5), 100 mM NaCl, 5 mM Na_3VO_4, 10 mM NaF, 10 μg/mL Leupeptin, 10 μg/mL pepstatinA, 1 mM DTT, and 10 mM $MgCl_2$, and incubated on ice for 15 min. After centrifuging at 20,000 × *g* for 15 min, supernatants were collected and applied to Protein A-Sepharose (GE Healthcare) conjugated with anti–Pan-Ras. After incubation for 30 min at 4 °C, Sepharose was extensively washed with lysis buffer containing 30 mM $MgCl_2$. Then, samples were eluted by boiling for 3 min in SDS/PAGE sample buffer and subjected to SDS/PAGE followed by Western blot analysis. For quantitative analysis of Western blots, intensity of individual bands was quantified using ImageJ software.

Transgenic and Knock-In Reporter Mice. We routinely determined the genotypes of offspring by genomic PCR using Taq DNA polymerase (New England Bio Labs) with primers listed in *SI Materials and Methods*. X-linked GFP mice (B6C3F1-Tg(CAG-EGFP)CX-FM038Osb) were provided by RIKEN BRC through the National Bio-Resource Project of the MEXT (Ministry of Education, Culture, Sports, Science, and Technology) , Japan and were described previously (26–28). To obtain the mice for genetic lineage tracing, we crossed SP-C-CreERT2 knock-in mice that were kindly donated by Brigit Hogan (Duke University, Durham, NC), with ROSA26-LacZ reporter mice, Gt(ROSA)26Sortm1Sor/J, obtained from the Jackson Laboratory.

Animal Treatment. For lineage tracing using SP-C-CreERT2 knock-in mice and ROSA26-LacZ reporter mice, the pups were administered subcutaneously with 4-OHT (0.1 mg/g) at P0 and P1. Inhibitors of MEK1/2 (PD0325901) (0.75 μg/2 g body weight per day) and MMP2 (MMP2 inhibitor III) (25 μg/g body weight per day) were formulated in 0.5% hydroxypropyl methylcellulose plus 0.2% Tween 80, as described previously (57), and injected into pups. To examine AMYF differentiation or number of alveoli, inhibitors were injected from P1 to P5 or from P1 to P14, respectively. To identify proliferating cells, BrdU (50 μg/g body weight) was intraperitoneally injected into the mice at P4. After 6 h, lungs were removed following perfusion with PBS and analyzed by immunohistochemistry. Protocols for mice were approved by the Institutional Animal Care and Use Committee of Chiba University.

ACKNOWLEDGMENTS. We thank Dr. Brigid Hogan (Duke University) and Dr. Masaru Okabe (Osaka University) for providing SP-C-CreERT2 knock-in mice and X-linked GFP mice, respectively. This work was supported by Grants-in-Aid for Young Scientists (B) (22790688), for the Japan Society for the Promotion of Science Fellows (24-5613), and for Challenging Exploratory Research (23659428) from the Japan Society for the Promotion of Science; Grants-in-Aid for Scientific Research on Priority Areas (20013007) and for Scientific Research on Innovative Areas (25117706) from the Ministry of Education, Culture, Sports, Science, and Technology; Intramural Research

Grant (23-5) for Neurological and Psychiatric Disorders of National Center of Neurology and Psychiatry; and grants from Kato Memorial Trust for Nambyo Research, Takeda Science Foundation, the Uehara Memorial Foundation, the Kishimoto Foundation, the Mochida Memorial Foundation, the Naito Foundation, and Astellas Foundation for Research on Metabolic Disorders.

1. Morrisey EE, Hogan BL (2010) Preparing for the first breath: Genetic and cellular mechanisms in lung development. *Dev Cell* 18(1):8–23.
2. Cardoso WV, Lü J (2006) Regulation of early lung morphogenesis: Questions, facts and controversies. *Development* 133(9):1611–1624.
3. Lindahl P, et al. (1997) Alveogenesis failure in PDGF-A-deficient mice is coupled to lack of distal spreading of alveolar smooth muscle cell progenitors during lung development. *Development* 124(20):3943–3953.
4. Boström H, et al. (1996) PDGF-A signaling is a critical event in lung alveolar myofibroblast development and alveogenesis. *Cell* 85(6):863–873.
5. Kimani PW, Holmes AJ, Grossmann RE, McGowan SE (2009) PDGF-Ralpha gene expression predicts proliferation, but PDGF-A suppresses transdifferentiation of neonatal mouse lung myofibroblasts. *Respir Res* 10:119.
6. McGowan SE, Grossmann RE, Kimani PW, Holmes AJ (2008) Platelet-derived growth factor receptor-alpha-expressing cells localize to the alveolar entry ring and have characteristics of myofibroblasts during pulmonary alveolar septal formation. *Anat Rec (Hoboken)* 291(12):1649–1661.
7. Burri PH (2006) Structural aspects of postnatal lung development—Alveolar formation and growth. *Biol Neonate* 89(4):313–322.
8. Schittny JC, Mund SI, Stampanoni M (2008) Evidence and structural mechanism for late lung alveolarization. *Am J Physiol Lung Cell Mol Physiol* 294(2):L246–L254.
9. Bourbon J, Boucherat O, Chailley-Heu B, Delacourt C (2005) Control mechanisms of lung alveolar development and their disorders in bronchopulmonary dysplasia. *Pediatr Res* 57(5 Pt 2):38R–46R.
10. Ambalavanan N, et al. (2008) Role of matrix metalloproteinase-2 in newborn mouse lungs under hypoxic conditions. *Pediatr Res* 63(1):26–32.
11. Atkinson JJ, et al. (2005) Membrane-type 1 matrix metalloproteinase is required for normal alveolar development. *Dev Dyn* 232(4):1079–1090.
12. Kheradmand F, Rishi K, Werb Z (2002) Signaling through the EGF receptor controls lung morphogenesis in part by regulating MT1-MMP-mediated activation of gelatinase A/MMP2. *J Cell Sci* 115(Pt 4):839–848.
13. Ding BS, et al. (2011) Endothelial-derived angiocrine signals induce and sustain regenerative lung alveolarization. *Cell* 147(3):539–553.
14. Shaw AT, et al. (2007) Sprouty-2 regulates oncogenic K-ras in lung development and tumorigenesis. *Genes Dev* 21(6):694–707.
15. Tang N, Marshall WF, McMahon M, Metzger RJ, Martin GR (2011) Control of mitotic spindle angle by the RAS-regulated ERK1/2 pathway determines lung tube shape. *Science* 333(6040):342–345.
16. Chang DR, et al. (2013) Lung epithelial branching program antagonizes alveolar differentiation. *Proc Natl Acad Sci USA* 110(45):18042–18051.
17. Roskoski R, Jr. (2012) ERK1/2 MAP kinases: Structure, function, and regulation. *Pharmacol Res* 66(2):105–143.
18. Roskoski R, Jr. (2012) MEK1/2 dual-specificity protein kinases: Structure and regulation. *Biochem Biophys Res Commun* 417(1):5–10.
19. Roskoski R, Jr. (2010) RAF protein-serine/threonine kinases: Structure and regulation. *Biochem Biophys Res Commun* 399(3):313–317.
20. Yokoyama T, et al. (2007) DA-Raf1, a competent intrinsic dominant-negative antagonist of the Ras-ERK pathway, is required for myogenic differentiation. *J Cell Biol* 177(5):781–793.
21. Kim KK, et al. (2006) Alveolar epithelial cell mesenchymal transition develops in vivo during pulmonary fibrosis and is regulated by the extracellular matrix. *Proc Natl Acad Sci USA* 103(35):13180–13185.
22. Kim Y, et al. (2009) Integrin alpha3beta1-dependent beta-catenin phosphorylation links epithelial Smad signaling to cell contacts. *J Cell Biol* 184(2):309–322.
23. Tanjore H, et al. (2009) Contribution of epithelial-derived fibroblasts to bleomycin-induced lung fibrosis. *Am J Respir Crit Care Med* 180(7):657–665.
24. Rock JR, et al. (2011) Multiple stromal populations contribute to pulmonary fibrosis without evidence for epithelial to mesenchymal transition. *Proc Natl Acad Sci USA* 108(52):E1475–E1483.
25. Soriano P (1999) Generalized lacZ expression with the ROSA26 Cre reporter strain. *Nat Genet* 21(1):70–71.
26. Kobayashi S, et al. (2006) Comparison of gene expression in male and female mouse blastocysts revealed imprinting of the X-linked gene, Rhox5/Pem, at preimplantation stages. *Curr Biol* 16(2):166–172.
27. Nakanishi T, et al. (2002) FISH analysis of 142 EGFP transgene integration sites into the mouse genome. *Genomics* 80(6):564–574.
28. Okabe M, Ikawa M, Kominami K, Nakanishi T, Nishimune Y (1997) 'Green mice' as a source of ubiquitous green cells. *FEBS Lett* 407(3):313–319.
29. Melendez-Zajgla J, Del Pozo L, Ceballos G, Maldonado V (2008) Tissue inhibitor of metalloproteinases-4. The road less traveled. *Mol Cancer* 7:85.
30. Murphy G (2011) Tissue inhibitors of metalloproteinases. *Genome Biol* 12(11):233.
31. Sato H, Takino T (2010) Coordinate action of membrane-type matrix metalloproteinase-1 (MT1-MMP) and MMP-2 enhances pericellular proteolysis and invasion. *Cancer Sci* 101(4):843–847.
32. Atkinson SJ, et al. (1995) Intermolecular autolytic cleavage can contribute to the activation of progelatinase A by cell membranes. *J Biol Chem* 270(51):30479–30485.
33. Rossello A, et al. (2004) New N-arylsulfonyl-N-alkoxyaminoacetohydroxamic acids as selective inhibitors of gelatinase A (MMP-2). *Bioorg Med Chem* 12(9):2441–2450.
34. Ebisuya M, Kondoh K, Nishida E (2005) The duration, magnitude and compartmentalization of ERK MAP kinase activity: Mechanisms for providing signaling specificity. *J Cell Sci* 118(Pt 14):2997–3002.
35. Pritchard CA, Bolin L, Slattery R, Murray R, McMahon M (1996) Post-natal lethality and neurological and gastrointestinal defects in mice with targeted disruption of the A-Raf protein kinase gene. *Curr Biol* 6(5):614–617.
36. Mikula M, et al. (2001) Embryonic lethality and fetal liver apoptosis in mice lacking the c-raf-1 gene. *EMBO J* 20(8):1952–1962.
37. Wojnowski L, et al. (1997) Endothelial apoptosis in Braf-deficient mice. *Nat Genet* 16(3):293–297.
38. Wiese S, et al. (2001) Specific function of B-Raf in mediating survival of embryonic motoneurons and sensory neurons. *Nat Neurosci* 4(2):137–142.
39. Galabova-Kovacs G, et al. (2006) Essential role of B-Raf in ERK activation during extraembryonic development. *Proc Natl Acad Sci USA* 103(5):1325–1330.
40. Huang W, Mabrouk ME, Sylvester J, Dehnade F, Zafarullah M (2011) Enhanced expression of tissue inhibitor of metalloproteinases-4 gene in human osteoarthritic synovial membranes and its differential regulation by cytokines in chondrocytes. *Open Rheumatol J* 5:81–87.
41. Young DA, et al. (2002) Identification of an initiator-like element essential for the expression of the tissue inhibitor of metalloproteinases-4 (Timp-4) gene. *Biochem J* 364(Pt 1):89–99.
42. Kim TS, Kim YB (1999) Correlation between expression of matrix metalloproteinase-2 (MMP-2), and matrix metalloproteinase-9 (MMP-9) and angiogenesis in colorectal adenocarcinoma. *J Korean Med Sci* 14(3):263–270.
43. Colarossi C, et al. (2005) Lung alveolar septation defects in Ltbp-3-null mice. *Am J Pathol* 167(2):419–428.
44. Neptune ER, et al. (2003) Dysregulation of TGF-beta activation contributes to pathogenesis in Marfan syndrome. *Nat Genet* 33(3):407–411.
45. Overall CM (2002) Molecular determinants of metalloproteinase substrate specificity: Matrix metalloproteinase substrate binding domains, modules, and exosites. *Mol Biotechnol* 22(1):51–86.
46. Srisuma S, et al. (2010) Fibroblast growth factor receptors control epithelial-mesenchymal interactions necessary for alveolar elastogenesis. *Am J Respir Crit Care Med* 181(8):838–850.
47. Weinstein M, Xu X, Ohyama K, Deng CX (1998) FGFR-3 and FGFR-4 function cooperatively to direct alveogenesis in the murine lung. *Development* 125(18):3615–3623.
48. Ad Hoc Statement Committee of the American Thoracic Society (2004) Mechanisms and limits of induced postnatal lung growth. *Am J Respir Crit Care Med* 170(3): 319–343.
49. Butler JP, et al. (2012) Evidence for adult lung growth in humans. *N Engl J Med* 367(3): 244–247.
50. Chen L, Acciani T, Le Cras T, Lutzko C, Perl AK (2012) Dynamic regulation of platelet-derived growth factor receptor α expression in alveolar fibroblasts during realveolarization. *Am J Respir Cell Mol Biol* 47(4):517–527.
51. Knudsen L, Weibel ER, Gundersen HJ, Weinstein FV, Ochs M (2010) Assessment of air space size characteristics by intercept (chord) measurement: An accurate and efficient stereological approach. *J Appl Physiol* 108(2):412–421.
52. Hsia CC, Hyde DM, Ochs M, Weibel ER; ATS/ERS Joint Task Force on Quantitative Assessment of Lung Structure (2010) An official research policy statement of the American Thoracic Society/European Respiratory Society: standards for quantitative assessment of lung structure. *Am J Respir Crit Care Med* 181(4):394–418.
53. Fehrenbach H, et al. (2008) Neoalveolarisation contributes to compensatory lung growth following pneumonectomy in mice. *Eur Respir J* 31(3):515–522.
54. Kim CF, et al. (2005) Identification of bronchioalveolar stem cells in normal lung and lung cancer. *Cell* 121(6):823–835.
55. Richards RJ, Davies N, Atkins J, Oreffo VI (1987) Isolation, biochemical characterization, and culture of lung type II cells of the rat. *Lung* 165(3):143–158.
56. Watanabe-Takano H, Takano K, Keduka E, Endo T (2010) M-Ras is activated by bone morphogenetic protein-2 and participates in osteoblastic determination, differentiation, and transdifferentiation. *Exp Cell Res* 316(3):477–490.
57. Ciuffreda L, et al. (2009) Growth-inhibitory and antiangiogenic activity of the MEK inhibitor PD0325901 in malignant melanoma with or without BRAF mutations. *Neoplasia* 11(8):720–731.